Thermal Pollution Monitoring of Tianwan Nuclear Power Plant for the Past 20 Years Based on Landsat Remote Sensed Data

Pingjing Nie, Hua Wu, Jie Xu, Letian Wei, Haitao Zhu, and Li Ni

***Abstract*—The Tianwan nuclear power plant is located in Jiangsu province of China. It discharges warm water from its cooling system into the Yellow Sea, which is bound to have ecological consequences. Herein, the changes in sea surface temperature (SST) after the operation of the Tianwan nuclear power plant were studied using Landsat data. First, the SST near the Tianwan nuclear power plant was estimated using a single-channel algorithm; subsequently, the datum temperature was extracted. Second, the area of thermal discharge was calculated. Finally, the thermal discharge was continuously monitored and analyzed, together with the overall trend of thermal discharge, its seasonal distribution characteristics, and the relationship between temperature rise and the impact of thermal discharge on the marine environment. Furthermore, there was no evident temperature pollution before the nuclear power plant was put into operation in May 2007; however, after the operation of the nuclear power plant, the thermally polluted area clearly expanded. An expansion of 66.77 km² was observed from 2001 to 2020 for areas experiencing higher temperatures. The largest thermally polluted area is observed in spring, followed by those in summer, winter, and autumn. In 2018, the temperature rise area in winter is 44.82 km² larger than that in autumn. The rise in SST at the Tianwan nuclear power plant meets the national quality standards for marine environments, and does not pollute the surrounding environment.**

***Index Terms*—Environmental function zones, Landsat, nuclear power station, remote sensing monitoring, seasonal distribution, temperature retrieving, thermal discharge.**

I. Introduction

THE nuclear power plant is a high-efficiency thermal power system that uses nuclear reactions as its thermal energy source. These plants emit almost negligible greenhouse gases and carbon dioxide, which indicates their great development potential that can address the issues of increasingly severe global greenhouse effect and limited resources. However, the thermal energy produced by nuclear power plants tends to discharge a significant amount of warm water into natural water bodies, which is known as thermal discharge. Accordingly, the temperature of the surrounding water environment increases, which may cause ecological problems [1]–[3]. For example, the potential impacts of thermal discharge on sea water include changes in hydrology, deterioration of sea water quality, deaths of sea animals that are sensitive to high temperature, and an increase in the frequency of red tides [4].

With the acceleration in the development of nuclear power in China, the problem of thermal discharge entering coastal water cannot be ignored [5]. Accordingly, there is a need for accurate monitoring and evaluation of the distribution range and degree of thermal drainage in nuclear power plants. Furthermore, monitoring the thermal discharge of nuclear power plants facilitates proper planning, increases nuclear energy use, and protects the marine environment [6], [7].

The traditional measurements of sea surface temperature (SST) are time-consuming and laborious, whereas data updates are slow and cannot cover all study areas. Aerial remoting sensing cannot provide easy-access data for a long term because it is an immature technology whose applicability is limited by certain airspace control regulations [5]. Space-based remote sensing technology is considered to be suitable for thermal discharge monitoring [8], [9] while exhibiting the advantages of dynamic continuity and a wide detection range [10]. Furthermore, it can monitor the changes in thermal discharge, provide references for environmental evaluation, and implement future planning of nuclear power plant construction.

Some researchers have used thermal infrared data derived from the Advanced Very High-Resolution Radiometer (AVHRR) with spatial resolution of 1.1 km to monitor the thermal discharge of nuclear power plants [11]. The HJ-1B thermal infrared data with spatial resolution of 300 m has also been used to monitor the thermal discharge of nuclear power plants [12]–[14]. In addition, several researchers have used Landsat data to monitor the thermal discharge of sea surface [5], [15].

Manuscript received May 2, 2021; revised May 23, 2021; accepted May 29, 2021. Date of publication June 11, 2021; date of current version June 28, 2021. This work was supported in part by the National High-Resolution Earth Observation Project of China under Grant 21-Y20B01-9001-19/22 and in part by the National Natural Science Foundation of China under Grants 41771398 and 41871267. *(Corresponding authors: Hua Wu; Haitao Zhu.)*

Pingjing Nie, Hua Wu, and Jie Xu are with the State Key Laboratory of Resources and Environmental Information System, Institute of Geographic Sciences and Natural Resources Research, Chinese Academy of Sciences, Beijing 100101, China, and also with the University of Chinese Academy of Sciences, Beijing 100049, China (e-mail: niepingjing19@mails.ucas.ac.cn; wuhua@igsnrr.ac.cn; xuj.19s@igsnrr.ac.cn).

Letian Wei is with the College of Resources and Environment, University of Chinese Academy of Sciences, Beijing 100049, China (e-mail: weiletian19@mails.ucas.ac.cn).

Haitao Zhu is with the Center for Satellite Application on Ecology and Environment, Ministry of Ecology and Environment, Beijing 100094, China (e-mail: zhuht@irsa.ac.cn).

Li Ni is with the Key Laboratory of Digital Earth Science, Aerospace Information Research Institute, Chinese Academy of Sciences, Beijing 100094, China (e-mail: nili@radi.ac.cn).

Digital Object Identifier 10.1109/JSTARS.2021.3088529

SST retrieval based on AVHRR and certain sensors is not sensitive to the temperature rise data of less than 1 km^2 because they exhibit a thermal infrared band resolution of approximately 1 km, whereas being unable to represent a thermally polluted area of less than 1 km^2 (such as the areas experiencing a temperature increase that exceeds 4°C and 5°C) [16].

Landsat satellites provide large and comprehensive data for monitoring nuclear power plants [5], [8], [9]. On March 1st, 1984, NASA launched Landsat 5 carried the multispectral scanner system and the thematic mapper (TM) instruments. Landsat 8 launched on February 11th, 2013 consisted of two instruments—the operational land imager and the thermal infrared sensor (TIRS). The resolutions of their Level 1 products (infrared data) have been used in this study after being resampled to 30 m, thereby rendering them ideal data sources for monitoring thermal discharge of nuclear power plants.

In previous studies, researchers have mostly used data for two to three years to study the distribution characteristics of thermal discharge in nuclear power plants [6], [11], [12], however, long-term changes in thermal pollution have not been tracked. Therefore, this article combined Landsat 5 and Landsat 8 data and selected 18 scenes with nearly clear sky and good data quality from 2001 to 2020. Subsequently, the single-channel method was used to retrieve the SST due to there being only one suitable TIR channel in the Landsat 5 and Landsat 8 satellites (band 11 exhibits serious calibration uncertainty). Then, the characteristics of the distribution of thermal discharge were analyzed, according to the thermal discharge map of the Tianwan nuclear plant. Finally, the areas of the Tianwan nuclear power plant, exhibiting different augmentations in temperatures for the past 20 years, were extracted.

The purpose of this article is to answer the following questions.

1) Does there exist an evident thermal discharge phenomenon?
2) How the area of thermal discharge changed from 2001 to 2020?
3) Are there any characteristics that indicate how the thermal distribution areas changed and what influences the distribution characteristics of the thermal discharge zone?
4) Does the rise in SST conform with the national quality standard for marine environments?

II. Study Area and Data

A. Study Area

The Tianwan nuclear power plant, which is located in China's Jiangsu Province, has been established as a result of a technical cooperation project between China and Russia (see Fig. 1). The plant area is planned to exhibit 8 million-kilowatt nuclear power units. Four 1.06 million kilowatt units (No.1, No.2, No.3, and No.4) have been built in the first and second phases of the project. The No.1 and 2 units were put into operation in 2007, which was followed by the operation of No.3 and 4 in 2018. The No.5 unit was put into operation in 2020, and No.6 unit has been planned to put into operation in October 2021. Meanwhile, No.7 and 8 are still being planned.

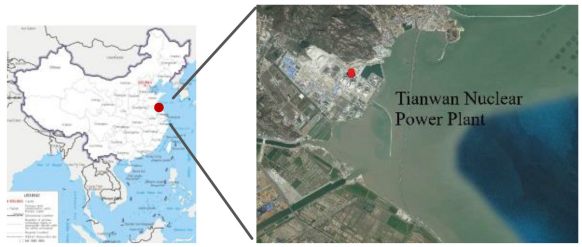

Fig. 1. Location of the Tianwan nuclear power plant.

The east side of the Tianwan nuclear power plant borders the Yellow Sea. The sea near the drainage outlet opens to the east like a semicircle, which leads to our study area being an east open gap ring-shaped harbor that has three closed sides.

B. Landsat Data

The Landsat program has offered over 50 years of consistently archived images of Earth's surface every 16 days since the early 1970s [17] with excellent quality, detail, coverage, and length. Landsat 5 carried the TM and Landsat 8 carried the TIRS. The Level 1 data derived using Landsat Collection 1 have been used in this study, which can be downloaded through the USGS website[1] free of charge.

Previous studies have shown that the thermal discharge of nuclear power plant is relevant to tide and season [5], [11], [13], [18]. Therefore, in this article, the 18 scenes that were chosen mostly exhibited cold seasons and similar tide characteristics to those observed during tidal fall; this ensures that the distribution features of thermal discharge are more evident [5], [13]. From 2001 to 2020, including the construction of the Tianwan nuclear power plant, a total of 18 Landsat scenes under nearly clear sky conditions were used in this study. The resolution of the used band is 30 m. Meanwhile, the path and row numbers of Landsat image data are 120 and 36, respectively, which cover the entire study area. The acquisition time of the Landsat data was listed in Table I.

III. Methodology

A. Procedure of Thermal Discharge Monitoring

The data processing method is based on the technological process of temperature drainage monitoring [14]. Meanwhile, SST is calculated by using the temperature retrieval process that employs the radiative transfer equation (RTE) method [19].

Fig. 2 shows the workflow of monitoring nuclear power plant thermal discharge based on remotely sensed Landsat data [14]. First, to determine the TOA radiance of an image, geometric correction and radiometric calibration were performed based on the raw digital number of the image. Then, the atmospheric correction, marine area extraction, and cloud recognition were implemented to obtain the TOA radiance images. The SST was retrieved based on the RTE. Afterward, the sea datum temperature was calculated, which was followed by the analysis of the

[1][Online]. Available: https://earthexplorer.usgs.gov/

TABLE I
INFORMATION RELATED TO LANDSAT 5/8 IMAGES

Satellite	Data acquisition time
Landsat5	2001-01-30
	2005-02-26
	2007-03-20
	2008-02-03
	2009-03-25
	2010-11-07
	2011-02-11
Landsat8	2013-11-15
	2014-07-29
	2015-03-10
	2016-01-08
	2017-02-11
	2018-01-13
	2018-04-19
	2018-06-06
	2018-10-28
	2019-04-16
	2020-03-23

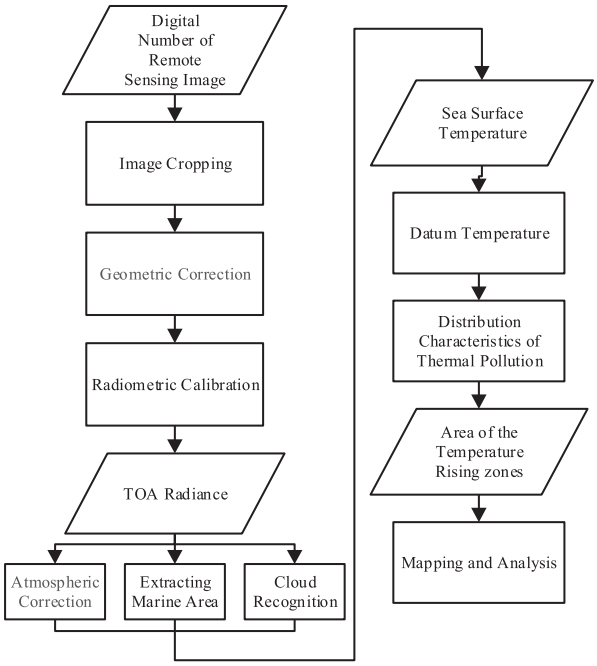

Fig. 2 Workflow of monitoring the thermal discharge of nuclear power plant based on remotely sensed Landsat data.

thermal distribution characteristics and thermal discharge zones. Finally, maps associated with thermal distributions of areas experiencing different temperature augmentations were produced for the Tianwan nuclear power plant from 2001 to 2020.

B. Data Preprocessing

The preprocessing of Landsat data mainly includes radiometric calibration and extraction of marine area. The equation used to convert the raw digital number of sensors to spectral radiance was as follows:

$$L_\lambda = DN \times G\mathrm{ain} + h \tag{1}$$

where L_λ represents radiance, DN is the raw digital number of the image, $G\mathrm{ain}$ is the coefficient of calibration, and h is the offset. The latter two parameters can be found in the Landsat metadata file. Indeed, the error of instrument calibration has a certain impact on the analysis of temperature spatiotemporal changes in this study. Barsi's research shows that the difference between the ETM+ and TIRS10 after calibrated is less than 0.78 W/(m^2·sr·μm) [2]. Besides, in 2017, the updates to the radiance-based absolute calibration of Landsat 5 TM and the stray light correction applied to Landsat 8 collection 1 level-1 data improve the accuracy of the absolute calibration. Vicarious calibration data over large water bodies were used to assess the stray light corrected image data. Initial results indicate significant improvement in the absolute accuracy of both TIRS bands. Errors were reduced from 2.1 K at 300 K with no correction to 0.3 K with the stray light correction for Band 10. Variability of these errors is reduced as well, from 0.87 K to 0.52 K at 300 K for Band 10 [3]. Moreover, this study focuses on the relative changes in SSTs, and it further weakens the influence of the uncertainty of calibration and temperature retrieval on the conclusions of temperature spatiotemporal changes in this article.

Subsequently, we used the marine region mask file to extract the ocean region in the ArcGIS 10.6 software [6]. Furthermore, the pixels contaminated by cloud were identified by the Landsat Quality Assurance band and were excluded from this article.

C. SST Retrieval

Since the Landsat 5 has only one thermal infrared channel [20], and the 11-band data of the Landsat 8 has a large calibration uncertainty [21], in this article, the single-channel algorithm was used to estimate the SST.

At present, there are three representative single-channel algorithms: the RTE method, mono-window [22], and generalized SC [23]. The main difference between the three algorithms is represented by the process of their atmospheric corrections [17]. Existing methods usually parameterize the atmospheric parameters as a function of total water or other parameters, which may cause systematic bias in the temperature retrieval process. Therefore, the MODTRAN is used in this manuscript to simulate the radiation transmission process. The MODTRAN-based radiation transmission simulation has great advantages in reducing the uncertainty in the process of atmospheric parameterization and improving the accuracy of temperature retrieval [24]. Many studies have proved that the RMSE of the radiative transmission equation-based single-channel algorithm in the retrieval of SST is within 1 K [25]. Therefore, this manuscript uses the RTE method to retrieve the temperature [26]–[29]. The sea surface emissivity in the thermal infrared spectrum is high and close to that of a black body [22]. Therefore, it can be calculated from the ASTER spectrum library[2].

[2][Online]. Available: https://earthexplorer.usgs.gov/

TABLE II
DETAILS OF THE NINE NDBC SITES AND LANDSAT

Lake location	West Superior	East Superior
Site ID	SPR_W	SPR_E
Longitude	89.793° W	86.585° W
Latitude	47.335° N	47.585° N
Elevation(m)	183	183
Buoy depth(m)	0.4	1.3
Anemometer height(m)	5.0	3.6
Sensor	Landsat8	Landsat8
Path/Row	25/27	23/27
Period	2013.4-2020.9	2014.8-2020.9

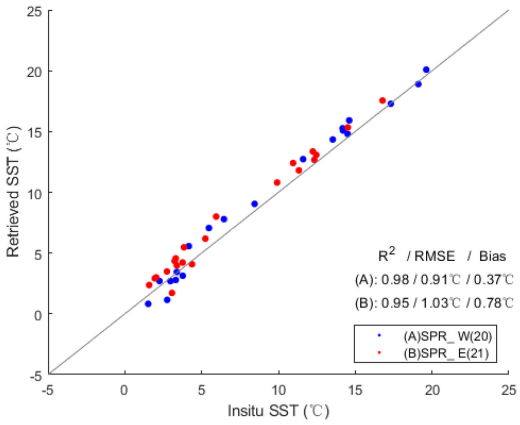

Fig. 3. Scatterplots of retrieval SST versus *in situ* SST at the two NDBC sites.

TABLE III
THERMAL DISCHARGE CLASSIFICATION

Thermal discharge level	Temperature range
+1 ℃	[1 ℃, 2 ℃)
+2 ℃	[2 ℃, 3 ℃)
+3 ℃	[3 ℃, 4 ℃)
+4 ℃	[4 ℃, 5 ℃)
+5 ℃	>5 ℃

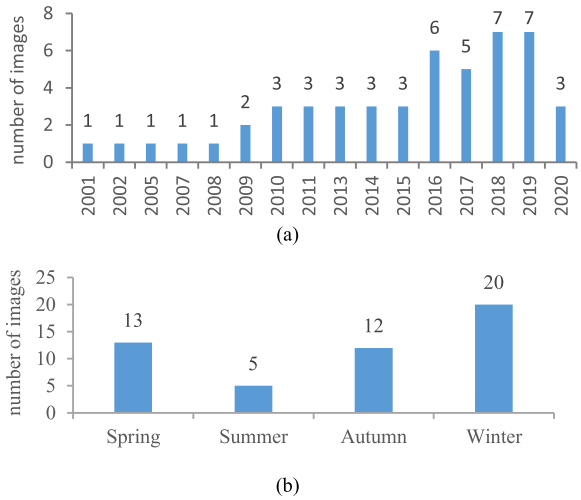

Fig. 4. Seasonal and year distribution of data.

D. SST Validation

Due to the lack of stations for SST observations near the study area, the *in situ* water temperature measurements collected at two sites in the Lakes Superior were used to evaluate the validity of the single-channel algorithm [30]. The temperature sensor was maintained by the National Data Buoy Center (NDBC). All data are quality-controlled and freely available[3]. Buoys are usually deployed in April or May and pulled out in October or November. Detailed information about the sites is provided in Table II.

According to the acquisition time of the measured data, we downloaded the remote sensing images around the site. After quality control, 20 and 21 images were selected from these two sites and the single-channel algorithm is used to estimate the water surface temperature. Furthermore, to compare with the skin temperature retrieved by satellite, bulk temperature measured by NDBC buoys at a certain depth should be converted to skin temperature [31], [32]. The method consists of three steps [33], using the bulk temperature, wind speed, anemometer height, and buoy depth to calculate daily averaged skin temperature, estimate the diurnal wave of skin temperature, and calculate the diurnal variation of skin temperature successively.

Fig. 3 shows the scatterplots of the SST retrieved versus *in situ* SST, and the R^2, RMSE, and Bias were calculated. The R^2 of Western and Eastern sites are 0.98 and 0.95, the Bias is 0.37 °C and 0.78 °C, and the RMSE is 0.91 °C and 1.03 °C, respectively, which shows that the single-channel algorithm used in this article has high accuracy in SST retrieval. In addition, this study focuses on the relative changes in SSTs, and it further weakens the influence of the uncertainty of calibration and temperature retrieval on the conclusions of temperature spatiotemporal changes.

[3][Online]. Available: https://www.ndbc.noaa.gov/

E. Datum Temperature Extracting and Thermal Discharge Classifying

Assuming that there is no heat drainage, the datum temperature, which is defined as the average temperature of the water surface, is mainly influenced by the thermal anomaly caused by the thermal discharge [14]. In this article, the average temperature correction method is used to extract the reference temperature of Tianwan area [5]. First, the average SST in the study area was calculated. Subsequently, the pixel in the discharge area whose temperature was 1 °C higher than the average temperature of whole water area of Tianwan Bay area was removed [8]. The temperature in the remaining areas is taken as the datum temperature. Consequently, the "threshold" method was used to extract the thermal discharge distribution zones of the nuclear power plant, which can be classified into five levels of thermal discharge [8], [14]: + 1 °C, + 2 °C, + 3 °C, + 4 °C, and > 5 °C; the detailed information has been listed in Table III.

IV. RESULTS AND DISCUSSION

A. Data Distribution

After eliminating the interference of factors that may affect the accuracy of SST retrievals, such as clouds and aerosols, a

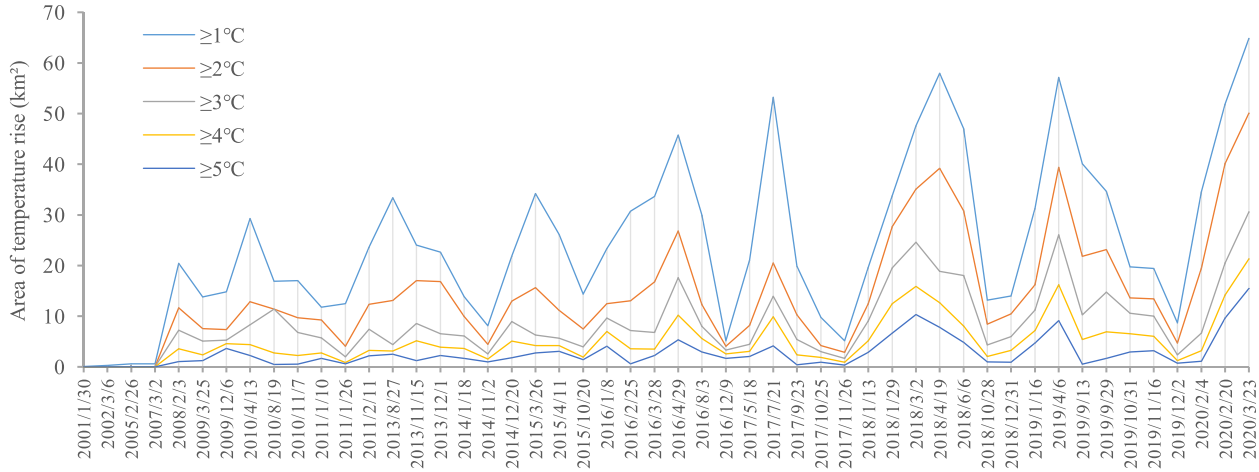

Fig. 5. Temperature rise area of different intensity from 2001 to 2020.

total of 50 images of Landsat from 2001 to 2020 were used in this article (see Fig. 4). Considering the No.1 nuclear power unit was put into use in May 2007, more images are used in recent years to analyze the status of thermal pollution of the Tianwan nuclear power plant [see Fig. 4(a)]. Judging from the seasonal distribution of available images, there are more Landsat images available in winter, accounting for about 41% of the total, and the smallest available images in summer, accounting for about 10%. This may be since the study area is in a monsoon climate zone, and the amount of available data decreased due to cloudy rain in summer.

According to the SST retrieved from satellite images, the different intensity of temperature rise areas of Tianwan nuclear power plants of whole data was calculated. As can be seen from Fig. 5, there are no obvious temperature rise zones in the research area before February 2008. The area of temperature rise shows a trend of increasing during the entire study period, and the seasonal characteristics are similar with a period of about one year. The temperature rise in spring and summer is higher than that in autumn and winter.

B. SST Before the Operation of the Nuclear Power Plant

There are three Landsat images that represent the period before the nuclear power plant was put into use in 2007. These three images are similar; therefore, only one of them has been shown in Fig. 6. It can be seen that the SST near the Tianwan nuclear power plant was mostly normal. A slight increase in the SST was observed near the land edge, which was considered to arise from the influence of mixed pixels in the land boundary area; therefore, it can be said that there was no obvious thermal discharge before the formal operation of the nuclear power plant.

C. SST Changes After the Operation of the Nuclear Power Plant

1) Increasing Trend of the Area Experiencing Temperature Augmentation: There are 15 images derived from Landsat that represent the operation of the nuclear power plant since 2007. Fig. 7 shows the distribution of areas in the Tianwan nuclear power plant that experience different temperature augmentations

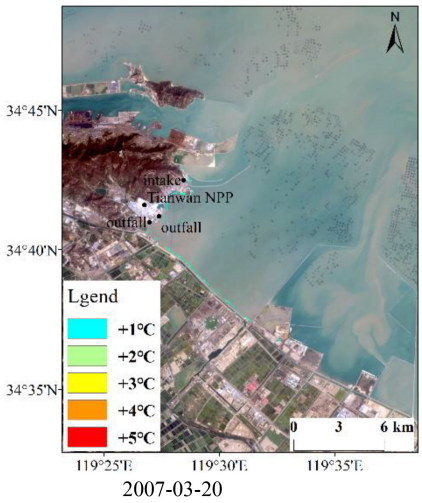

Fig. 6. Distribution of the area experiencing temperature augmentations before the operation of the Tianwan nuclear power plant.

from 2008 to 2020. These areas are located in the northeast or southeast of the drainage outlet of the Tianwan nuclear power plant. The temperature rise near the drain is observed to be the highest; however, in areas that are farther away from the drain, the rate of rising in temperature gradually decreases due to dilution and cooling of seawater. Table IV presents the thermal discharge areas with different levels of temperature augmentations.

The thermal discharge area (exceeding 1 °C rise) in 2008 was 20.45 km², whereas that in 2020 was 64.84 km² (see Fig. 7). We can observe that the area experiencing thermal pollution is gradually expanding.

The images in Fig. 7 also show that the distribution characteristics of thermal discharge over time are different, including the diffusion direction, offshore distance, distribution shape, and temperature gradient between different levels of temperature rise; these varying characteristics may be the reason for tide formation.

Whenever a falling tide is observed [for example, on February 27, 2017 [Fig. 7(i)] and January 8, 2016 [Fig. 7(h)]], the tidal

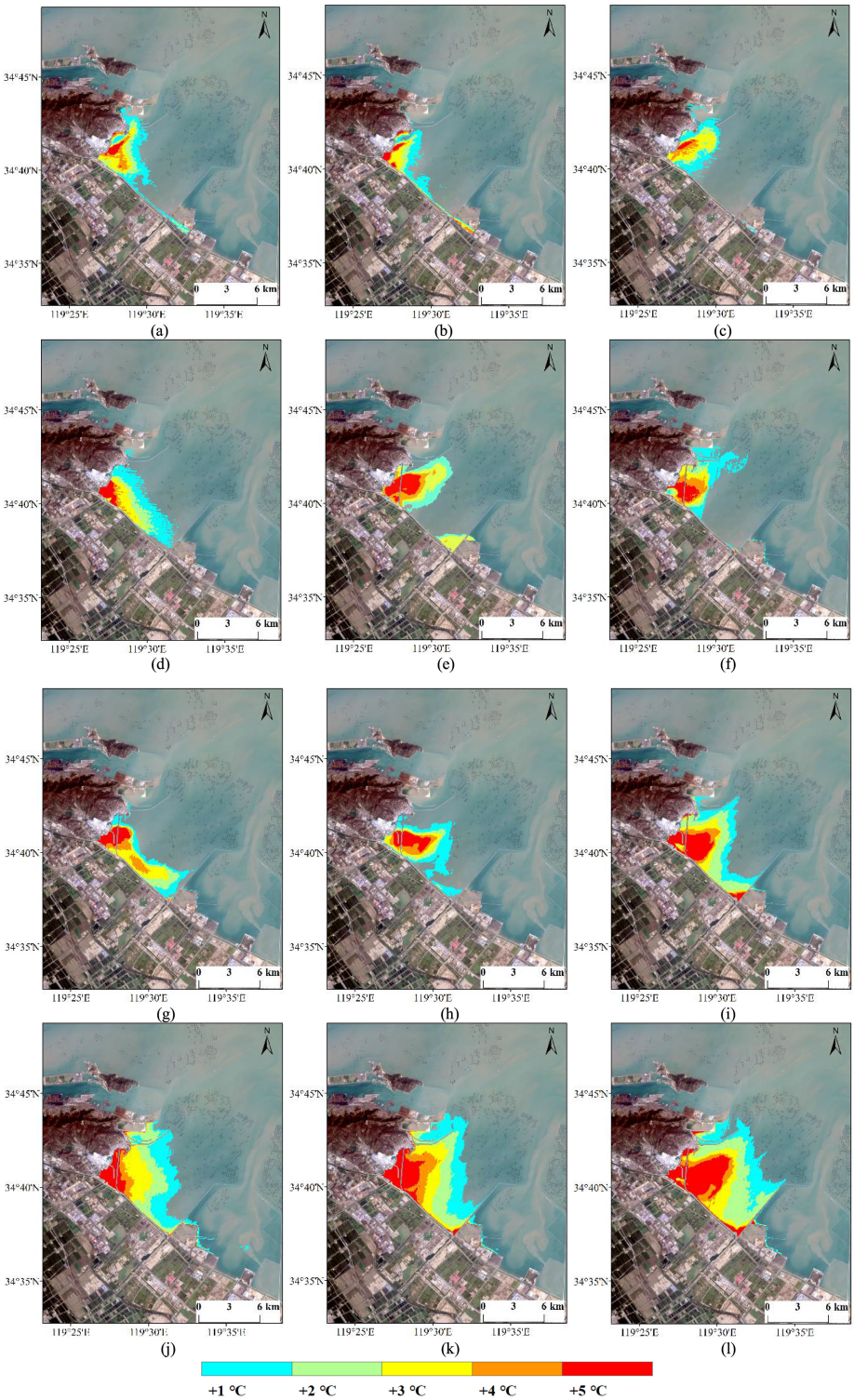

Fig. 7. Distribution of the area experiencing temperature augmentations during the operation of the Tianwan nuclear power plant. (a) 2008-02-03. (b) 2009-03-25. (c) 2010-11-07. (d) 2011-02-11. (e) 2013-11-15. (f) 2014-07-29. (g) 2015-03-10. (h) 2016-01-08. (i) 2017-02-27. (j) 2018-06-06. (k) 2019-04-06. (l) 2020-03-23.

current direction is the same as the diffusion direction of the thermal discharge, which helps the thermal discharge spread toward the open sea; it is usually distributed in the east or northeast direction. The falling tide pushes the thermal discharge away from the shore; the thermal discharge distribution is fan-shaped or oval, and the temperature gradient between different grades of temperature augmentations decreases.

Whenever the tide rises [for example, on February 11, 2011 [Fig. 7(d)] and March 10, 2015 [Fig. 7(g)]], the direction of the tidal current movement is opposite to the diffusion direction

TABLE IV
STATISTICS OF THERMAL DISCHARGE AREA WITH DIFFERENT LEVELS

Time	Area (km^2)				
	+1 ℃	+2 ℃	+3 ℃	+4 ℃	+5 ℃
2008/2/3	8.79	4.45	3.65	2.49	1.07
2009/3/25	6.22	2.50	2.72	1.15	1.21
2010/11/7	7.33	2.89	4.57	1.7	0.52
2011/02/11	11.34	4.94	4.13	1.12	2.15
2013/11/15	7.00	8.51	3.41	3.87	1.26
2014/7/29	8.98	2.85	2.98	3.32	2.96
2015/3/10	5.73	4.17	5.54	3.53	3.21
2016/1/8	10.84	2.85	2.66	2.92	4.06
2017/2/27	9.82	11.44	4.6	3.24	8.23
2018/6/6	16.22	12.75	10.03	3.21	4.82
2019/4/6	17.76	13.32	9.9	7.03	9.15
2020/3/23	14.76	19.49	9.28	5.84	15.47

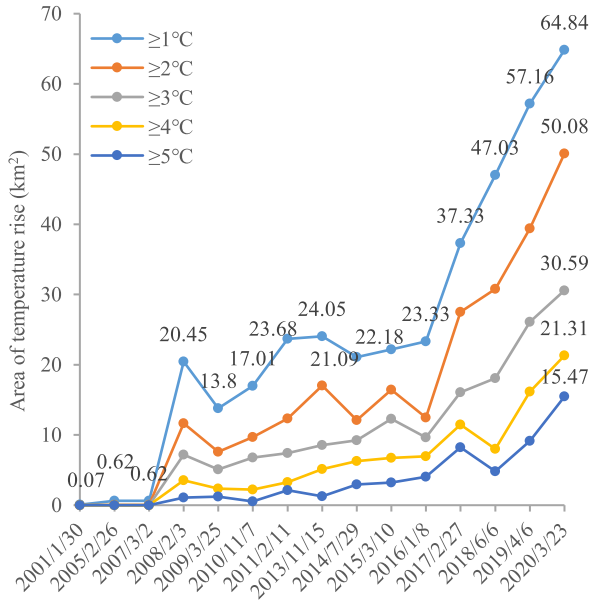

Fig. 8. Trends of different intensities of thermally polluted areas in Tianwan nuclear power plant.

of thermal discharge, and the thermal discharge distribution is squeezed by the sea currents. The coastal edge is distributed toward the southeast of the outfall, whereas the distribution shape becomes narrower and longer in the form of a long strip or rectangle. The temperature gradient between different grades of temperature augmentations increases.

Fig. 8 indicates the largest area that experiences temperature augmentations from 2001 to 2020. The zones showing a temperature increase of above 1 °C increased in area by 64.77 km²; however, the zones exhibiting a temperature increase of above 4 °C increased in area by 21.31 km². This result shows that the area of the Tianwan nuclear power plant, which experiences temperature augmentations, changed with a wavy upward trend since 2001. The change curve from 2008 to 2016 was flatter. After 2017, the areas experiencing temperature augmentations showed a near-linear growth. The areas experiencing a lower temperature rise tend to increase faster than those experiencing a higher temperature rise.

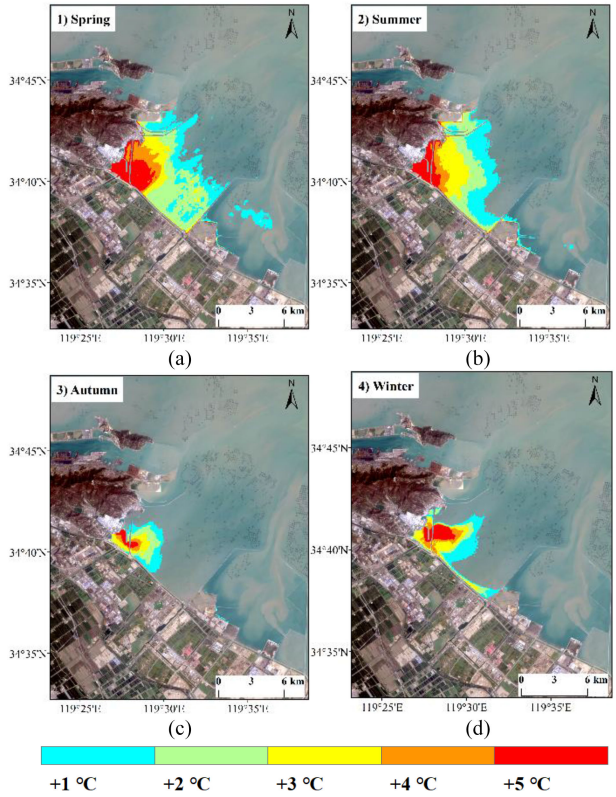

Fig. 9. Seasonal distributions of the rise in temperature of the thermal discharge. (a) 2018-04-19. (b) 2018-06-06. (c) 2018-10-28. (d) 2018-01-13.

2) Seasonal Variation in Areas Experiencing Temperature Augmentations: Fig. 9 shows that in spring and summer, the thermal discharge spreads around the outfall, and extends toward the southeast and northeast when it hits the coast. Further, the thermal discharge area is large and distributed far from the coast, especially in spring. In autumn and winter, the thermal discharge is close to the drainage outlet; however, its distribution is significantly smaller. Moreover, the thermal discharge areas are mixed in spring, whereas zone boundaries of different thermal discharge levels are clearer in other seasons. In summer, the gradient associated with the temperature drop at different thermal discharge level zones is the smallest.

Fig. 10 shows that the higher the intensity of the rise in temperature, the smaller the area experiencing this rise; this is true for each season. For each intensity of the rise in temperature, the largest thermally polluted area is observed in spring, followed by those in summer, winter, and autumn. The difference among the thermal distributions is the largest when the temperature increases by above 1 °C, whereas it is the smallest when the temperature increases by above 5 °C.

D. Relationship Between the Range of the Rise in Temperature and Coastal Environment Function Zones

The coastal marine environment function zone of the Tianwan sea area is shown in Fig. 11, according to the relevant documents of the Chinese government ("The requirements of the Letter on the Approval of the Adjustment of Environmental Function Zoning in the Nearby of Lianyungang Tianwan Nuclear Power

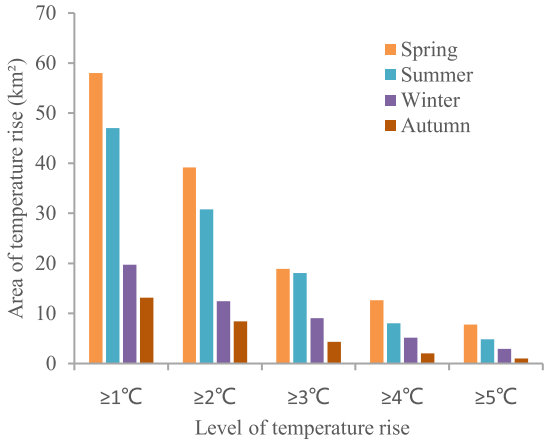

Fig. 10. Statistical representation of areas experiencing varying temperature augmentations in different seasons.

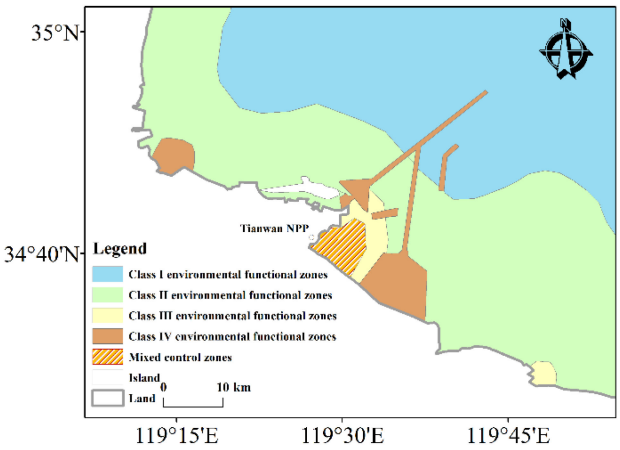

Fig. 11. Coastal marine environment function zone.

Station" (Suhuan Committee Office [2015] No.27)). The control area where different thermal discharges of the Tianwan nuclear power plant are mixed is 44.9 km², and the SST in this area does not need to comply with the national seawater quality standard. However, seawater quality standards must be met for the rest of the region. Seawater Quality National Standard (GB 3097-1997) states that for the sea water quality in Class I and Class II environmental functional zones, the man-made rise in sea water temperature should not exceed 1 °C in summer and 2 °C in other seasons; for sea water quality in Class III and Class IV environmental functional zones, the man-made rise in sea water temperature should not exceed 4 °C.

The remote sensing monitoring results of 18 images from 2001 to 2020 were overlapped and displayed in Fig. 12; these results were then compared with the environmental functional areas near the nuclear power plant. Fig. 12 shows that all the areas experiencing temperature augmentations, which exceed 4 °C near the outfall of the nuclear power plant, are in the mixed control zone. However, SST in the mixing zone does not need to meet the seawater quality standard.

A small part of the area experiencing temperature augmentations that exceed 5 °C is distributed in the outfall of the nuclear power plant in the land boundary area of the southeast sea. Furthermore, multiple images were collected when the tides fell

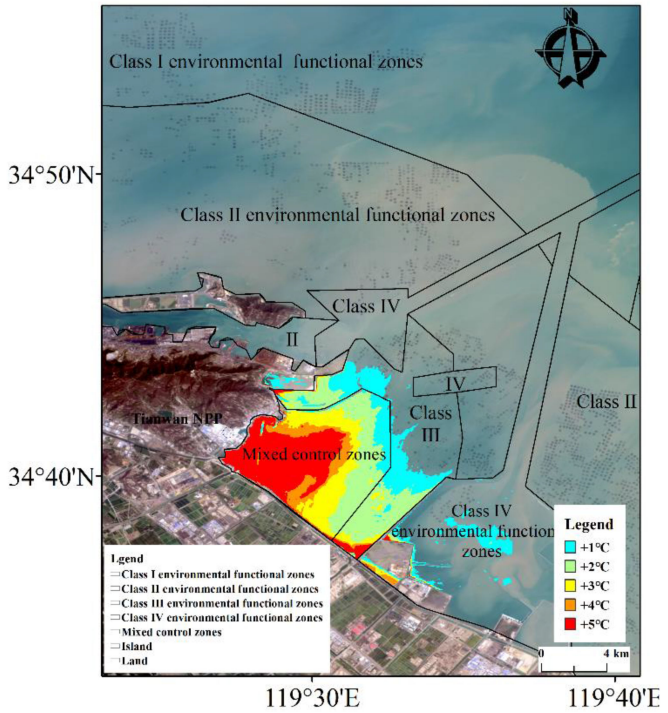

Fig. 12. Comparison of thermal discharge and environmental function zones of the Tianwan nuclear power plant.

on the sea water flow overseas, thereby exposing the dry beach on the shore. The dry beach temperature was much higher than the sea water temperature, which leads to an increase in temperature that exceeds 5 °C in this area. Fig. 12 also shows that the area experiencing temperature augmentations exceeding 1 °C is in the range of Class III or Class IV environmental functional zones, but not in the range of Class I or Class II functional zones. However, the temperature rise is in the range of Class III functional zones (1 °C and 2 °C). The small areas that experience temperature augmentations in excess of 4 °C within Class III area are also considered to be located in the dry beach. Therefore, the temperature rise in the environmental function zone meets the national quality standards for marine environments.

In conclusion, the SST rises in the Tianwan nuclear power plant; however, it generally meets the national quality standards for marine environments, and does not cause pollution to the surrounding environment.

V. Summary and Conclusion

This research studied the thermal discharge of the Tianwan nuclear power plant. The pollution analysis was based on the comparison of the water temperature with the surrounding environment. The temperature of the sea surface was retrieved by using the single-channel algorithm with the Landsat data. Furthermore, this study elucidated that the area of thermal discharge changed from 2001 to 2020.

1) Before the nuclear power plant was put into operation, the SST was mostly normal near the Tianwan nuclear power plant; hence, there was no thermal pollution. After the operation of the nuclear power plant, it can be clearly observed that the thermally polluted area expanded.

2) The areas experiencing temperature augmentations show an increasing trend overall. From 2001 to 2020, the areas that exhibit a rise in temperature increased by 66.77 km². The maximum increase in area was observed for temperature augmentations above 2 °C (19.49 km²), whereas the minimum increase was observed for augmentations above 4 °C (5.84 km²).
3) The areas experiencing temperature augmentations also change seasonally. The largest thermally polluted area is observed in spring, followed by those in summer, winter, and autumn.
4) The SST rise in the Tianwan nuclear power plant meets the national quality standards for marine environments, and does not cause pollution to the surrounding environment. Therefore, the construction of other nuclear power plant units can be continued in the future.

The results of monitoring temperature changes in nuclear power plants using remotely sensed data can provide references to study the thermal discharges of nuclear power plants and their environmental impacts. Landsat dataset provides suitable remote sensing data to study the thermal discharge of the Tianwan nuclear power plant. These results can serve as useful information for assessing the impact of nuclear power plants on their future planning and surrounding environment. However, datum temperature extraction will influence the analysis of the thermal discharge of the nuclear power plant. In a future study, more attention will be paid to the extraction method used for datum temperature.

References

[1] J. Yu, D. Tang, L. Yao, P. Chen, X. Jia, and C. Li, "Long-term water temperature variations in Daya Bay, China using satellite and in situ observations," *Terr. Atmos. Ocean. Sci.*, vol. 21, no. 2, pp. 393–399, Apr. 2010.

[2] F. Verones, M. M. Hanafiah, S. Pfister, M. A. J. Huijbregts, G. I. Pelletier, and A. J. E. S. Koehler, "Characterization factors for thermal pollution in freshwater aquatic environments," *Environ. Sci. Technol.*, vol. 44, no. 24, pp. 9364–9369, 2010.

[3] W. Zhao, J. He, Y. Wu, D. Xiong, F. Wen, and A. Li, "An analysis of land surface temperature trends in the central Himalayan region based on MODIS products," *Remote Sens.*, vol. 11, no. 8, 2019, Art. no. 900.

[4] X. Huang, X. Chen, X. Peng, R. Zhang, X. Qian, and J. Tang, "Research progress on the impact of warm drainage on marine environment in coastal power plants," *Mar. Environ. Sci.*, vol. 33, no. 6, pp. 972–976, Dec. 2014.

[5] X. Zhang, J. Xu, M. Zhang, and J. Li, "Distribution of thermal discharge from Tianwan nuclear power plant: Analysis of thermal infrared data from Landsat," *Adv. Mar. Sci.*, vol. 37, no. 3, pp. 518–525, Jul. 2019.

[6] X. Wang, X. Su, X. Wang, L. Wang, and S. Wen, "Thermal plume monitoring of Hongyanghe nuclear power plant based on Landsat-8 satellite data," *Infrared*, vol. 36, no. 8, pp. 50–56, Jul. 2015.

[7] K. Wei *et al.*, "Reflections on the Catastrophic 2020 Yangtze river basin flooding in Southern China," *Innovation*, vol. 1, no. 2, 2020, Art. no. 100038.

[8] C. Chen, P. Shi, and Q. Mao, "Application of remote sensing techniques for monitoring the thermal pollution of cooling-water discharge from nuclear power plant," *Environ. Lett.*, vol. 38, no. 8, pp. 1659–1668, Aug. 2003.

[9] A. Thomas, D. Byrne, and R. Weatherbee, "Coastal sea surface temperature variability from Landsat infrared data," *Remote Sens. Environ.*, vol. 81, no. 2/3, pp. 262–272, 2002.

[10] L. Zhu *et al.*, "Monitoring the thermal plume from coastal nuclear power plant using satellite remote sensing data modeling and validation," *Spectrosc. Spectral Anal.*, vol. 34, no. 11, pp. 3079–3084, Nov. 2014.

[11] D. Tang, D. R. Kester, Z. Wang, J. Lian, and H. Kawamura, "AVHRR satellite remote sensing and shipboard measurements of the thermal plume from the Daya Bay, nuclear power station, China," *Remote Sens. Environ.*, vol. 84, no. 4, pp. 506–515, 2003.

[12] J. Xu, L. Zhu, J. Jiang, J. Li, S. Zhao, and L. Yuan, "Monitoring thermal discharge in Daya Bay plant based on the thermal infrared band of HJ-1B and TM remote sensing data," *China Environ. Sci.*, vol. 34, no. 5, pp. 1181–1186, 2014.

[13] Y. Zhou, C. Gong, Y. Hu, and Q. Chen, "Distribution of thermal discharge from a power station based on HJ-1B and FY-3 thermal infrared data," *Proc. SPIE*, vol. 8193, 2011, Art. no. 819330.

[14] L. Zhu *et al.*, "Remote sensing monitoring of thermal discharge in Daya Bay nuclear power station based on HJ-1 infrared camera," *Proc. SPIE*, vol. 9261, 2014, Art. no. 92610V.

[15] Y. H. Ahn, P. Shanmugam, J. H. Lee, and Y. Q. Kang, "Application of satellite infrared data for mapping of thermal plume contamination in coastal ecosystem of Korea," *Mar. Environ. Res.*, vol. 61, no. 2, pp. 186–201, 2006.

[16] Y. Zhou, C. Gong, D. B. Kuang, and Y. Hu, "Distribution of thermal discharge from a power plant: Analysis of thermal infrared data from the environmental mitigation satellite," *J. Infrared Millimeter Terahertz Waves*, vol. 31, no. 6, pp. 544–549, Dec. 2012.

[17] M. Wang, Z. Zhang, T. Hu, and X. Liu, "A practical single-channel algorithm for land surface temperature retrieval: Application to Landsat series data," *J. Geophys. Res.-Atmos.*, vol. 124, no. 1, pp. 299–316, 2019.

[18] M. Liu, X. Yin, Q. Xu, Y. Chen, and B. Wang, "Monitoring of fine-scale warm drain-off water from nuclear power stations in the Daya Bay based on Landsat 8 data," *Remote Sens.*, vol. 12, no. 4, Feb. 2020, Art. no. 627.

[19] A. Sekertekin, "Validation of physical radiative transfer equation-based land surface temperature using Landsat 8 satellite imagery and SURFRAD in-situ measurements," *J. Atmos. Sol.-Terr. Phys.*, vol. 196, 2019, Art. no. 105161.

[20] M. A. Wulder *et al.*, "Current status of Landsat program, science, and applications," *Remote Sens. Environ.*, vol. 225, pp. 127–147, May 2019.

[21] J. C. Jimenez-Munoz, J. A. Sobrino, D. Skokovic, C. Mattar, and J. Cristobal, "Land surface temperature retrieval methods from Landsat-8 thermal infrared sensor data," *IEEE Geosci. Remote Sens. Lett.*, vol. 11, no. 10, pp. 1840–1843, Oct. 2014.

[22] Z. Qin, A. Karnieli, and P. Berliner, "A mono-window algorithm for retrieving land surface temperature from Landsat TM data and its application to the Israel-Egypt border region," *Int. J. Remote Sens.*, vol. 22, no. 18, pp. 3719–3746, Dec. 2001.

[23] J. A. Sobrino, J. C. Jiménez-Muñoz, and L. Paolini, "Land surface temperature retrieval from LANDSAT TM 5," *Remote Sens. Environ.*, vol. 90, no. 4, pp. 434–440, 2004.

[24] J. Yang *et al.*, "Evaluation of seven atmospheric profiles from reanalysis and satellite-derived products: Implication for single-channel land surface temperature retrieval," *Remote Sens.*, vol. 12, no. 5, Mar. 2020, Art. no. 791.

[25] X. Yu, X. Guo, and Z. Wu, "Land surface temperature retrieval from Landsat 8 TIRS—Comparison between radiative transfer equation-based method, split window algorithm and single channel method," *Remote Sens.*, vol. 6, no. 10, pp. 9829–9852, Oct. 2014.

[26] M. Wang, Z. Zhang, G. He, G. Wang, T. Long, and Y. Peng, "An enhanced single-channel algorithm for retrieving land surface temperature from Landsat series data," *J. Geophys. Res., Atmos.*, vol. 121, no. 19, pp. 11712–11722, 2016.

[27] M. Pivovarnik, S. J. S. Khalsa, J. C. Jimenez-Munoz, and F. Zemek, "Improved temperature and emissivity separation algorithm for multispectral and hyperspectral sensors," *IEEE Trans. Geosci. Remote Sens.*, vol. 55, no. 4, pp. 1944–1953, Apr. 2017.

[28] F. Wang, Z. Qin, C. Song, L. Tu, A. Karnieli, and S. Zhao, "An improved mono-window algorithm for land surface temperature retrieval from Landsat 8 thermal infrared sensor data," *Remote Sens.*, vol. 7, no. 4, pp. 4268–4289, Apr. 2015.

[29] X. Yang and P. Huang, "Restored relationship between ENSO and Indian summer monsoon rainfall around 1999/2000," *Innovation*, vol. 2, no. 2, 2021, Art. no. 100102.

[30] S.-B. Duan *et al.*, "Validation of Landsat land surface temperature product in the conterminous United States using in situ measurements from SURFRAD, ARM, and NDBC sites," *Int. J. Digit. Earth*, vol. 14, no. 5, pp. 640–660, 2020.

[31] C. W. Fairall, E. F. Bradley, J. S. Godfrey, G. A. Wick, J. B. Edson, and G. S. Young, "Cool-skin and warm-layer effects on sea surface temperature," *J. Geophys. Res., Oceans*, vol. 101, no. C1, pp. 1295–1308, 1996.

[32] W. Zhao, D. Xiong, F. Wen, and X. Wang, "Lake area monitoring based on land surface temperature in the Tibetan Plateau from 2000 to 2018," *Environ. Res. Lett.*, vol. 15, no. 8, 2020, Art. no. 084033.

[33] X. Zeng, M. Zhao, R. E. Dickinson, and Y. He, "A multiyear hourly sea surface skin temperature data set derived from the TOGA TAO bulk temperature and wind speed over the tropical Pacific," *J. Geophys. Res., Oceans,* vol. 104, no. C1, pp. 1525–1536. 1999.

Pingjing Nie received the B.S. degree in geographic information systems from the Honors College of Henan Polytechnic University, Jiaozuo, China, in 2019. She is currently working toward the master's degree with the State Key Laboratory of Resources and Environmental Information System, Institute of Geographic Sciences and Natural Resources Research, Chinese Academy of Sciences, Beijing, China.

Her research interests include temperature retrieval and application.

Hua Wu received the B.S. degree in photogrammetric engineering and remote sensing from Wuhan University, Wuhan, China, in 2003, the M.S. degree in cartography and geographical information system from Beijing Normal University, Beijing, China, in 2006, and the Ph.D. degree in cartography and geographical information system from the Institute of Geographic Sciences and Natural Resources Research, Chinese Academy of Sciences (CAS), Beijing, in 2010.

He is currently a Professor with the Institute of Geographic Sciences and Natural Resources Research, CAS. His research interests include the retrieval, validation, and scaling of remotely sensed products.

Jie Xu received the B.S. degree in geographic information systems from the Honors College of Henan Polytechnic University, Jiaozuo, China, in 2019. He is currently working toward the master's degree with the State Key Laboratory of Resources and Environmental Information System, Institute of Geographic Sciences and Natural Resources Research, Chinese Academy of Sciences, Beijing, China.

His research interests include remote sensing and environmental monitoring.

Letian Wei received the B.S. degree in geography science from the Honors College of Zhejiang Normal University, Jinhua, China, in 2019. She is currently working toward the master's degree in cartography and geographical information system with the College of Resources and Environment, University of Chinese Academy of Sciences, Beijing, China.

Her research interests include remote sensing quantitative calculation and modeling.

Haitao Zhu received the B.S. degree in land resources management from the Chengdu University of Technology, Chengdu, China, in 2010, and the M.S. degree in electronics and communication engineering from the Institute of Remote Sensing and Digital Earth, Chinese Academy of Sciences, Beijing, China, in 2013.

He is currently an Engineer with Center for the Satellite Application on Ecology and Environment, Ministry of Ecology and Environment, Beijing. His research interests include the remote sensing of ecology and environment and the application of UAV remote sensing.

Li Ni received the Ph.D. degree in cartography and geographical information system from the Institute of Remote Sensing and Digital Earth, Chinese Academy of Sciences, Beijing, China, in 2015.

She is currently an Associate Researcher with the Aerospace Information Research Institute, Chinese Academy of Sciences. Her research interests include the land surface temperature retrieval and application of hyperspectral remote sensing.